

MAJOR PAPER

Thin-slice Free-breathing Pseudo-golden-angle Radial Stack-of-stars with Gating and Tracking T_1 -weighted Acquisition: An Efficient Gadoteric Acid-enhanced Hepatobiliary-phase Imaging Alternative for Patients with Unstable Breath Holding

Kimihiko Kajita¹, Satoshi Goshima^{1*}, Yoshifumi Noda¹, Hiroshi Kawada¹,
Nobuyuki Kawai¹, Tomoyuki Okuaki², Masatoshi Honda², and Masayuki Matsuo¹

Purpose: To compare four free-breathing scan techniques for gadoteric acid-enhanced hepatobiliary phase imaging with conventional breath-hold scans.

Materials and Methods: Gadoteric acid-enhanced hepatobiliary phase imaging with six image acquisition sets performed in 50 patients. Image acquisition sets included fat-suppressed 3D T_1 -weighted turbo field echo with free-breathing pseudo-golden-angle radial stack-of-stars (FBRS) acquisition, FBRS with track (FBRS_T), FBRS with gate and track (FBRS_{G&T}), thin-slice FBRS with gate and track (thin-slice FBRS_{G&T}), free-breathing Cartesian acquisition (Cartesian_{FB}), and breath-hold Cartesian acquisition (Cartesian_{BH}). Signal-to-noise ratio (SNR), contrast-to-noise ratio (CNR), and image quality compared to the six-image acquisition sets.

Results: Signal-to-noise ratio and CNR were significantly higher in FBRS, FBRS_T, FBRS_{G&T} and thin-slice FBRS_{G&T} than in Cartesian_{FB} and Cartesian_{BH} ($P < 0.001$). Based on sharpness, motion artifacts, visibility of intrahepatic vessels, and overall image quality, thin-slice FBRS_{G&T} had the highest image quality followed by Cartesian_{BH} and FBRS_{G&T} ($P < 0.001$). Severe motion artifacts were observed in 25 patients in Cartesian_{FB} and three patients in Cartesian_{BH}, whereas image quality remained above the acceptable range in FBRS_{G&T}, FBRS_T, FBRS, and thin-slice FBRS_{G&T} in all cases.

Conclusion: Thin-slice FBRS_{G&T} demonstrated excellent image quality compared with conventional Cartesian_{BH} in gadoteric acid-enhanced hepatobiliary phase imaging. It can be apply to supplemental sequences of patients with unstable breath holding.

Keywords: *free-breathing, Gadoteric acid, hepatobiliary phase, magnetic resonance imaging*

Introduction

Gadoteric acid-enhanced MRI is widely used in routine clinical practice.^{1,2} The gadoteric acid contrast medium is taken up by hepatocytes via the membrane transporter.^{3,4} Subsequently, liver-specific contrast-enhanced phase (hepatobiliary phase) is obtained 20 min after the injection.⁵ Hepatobiliary phase imaging produces exceptional contrast resolution for liver parenchyma, which enables excellent differentiation

between lesions with and without functional hepatocytes.⁶ Recent technical innovations have improved the acquisition of liver MRI. The routine liver MRI protocol consists of unenhanced T_1 -, T_2 -, and diffusion-weighted imaging followed by gadoteric acid-enhanced dynamic and hepatobiliary phase imaging.^{7,8} In the last few years, the development of fat-suppressed 3D T_1 -weighted gradient-echo imaging has contributed to gadoteric acid-enhanced imaging with a thinner effective slice thickness.⁷ However, image quality in breath-hold sequences is seriously impaired in some patients, such as the elderly and those with ascites, hearing loss, and tremors, because of unstable breath holding.

The free-breathing radial k -sampling technique has recently been developed and has been applied in clinical settings.^{9–11} We hypothesized that the use of free-breathing liver-imaging acquisition techniques may contribute to the improvements of image quality and spatial resolution during

¹Department of Radiology, Gifu University, 1-1 Yanagido, Gifu 501-1194, Japan
²Philips Healthcare, Tokyo, Japan

*Corresponding author, Phone: +81-58-230-6439, Fax: +81-58-230-6440,
E-mail: gossy@par.odn.ne.jp

©2018 Japanese Society for Magnetic Resonance in Medicine
This work is licensed under a Creative Commons Attribution-NonCommercial-NoDerivatives International License.

Received: September 29, 2017 | Accepted: February 7, 2018

gadoteric acid-enhanced hepatobiliary phase imaging. Thus, this study aimed to assess four scan techniques with free-breathing pseudo-golden-angle radial stack-of-stars (FBRS) acquisition for gadoteric acid-enhanced hepatobiliary phase imaging compared with the conventional Cartesian acquisition technique.

Materials and Methods

Patients

This prospective study was approved by the institutional review board (Gifu University, Gifu, Japan) and written informed consent was obtained from all patients. We included the patients received gadoteric acid-enhanced MRI from November 2016 to January 2017. We excluded the patients with status post-hepatectomy and numerous hepatic masses because these situations cause anomalous signal changes on the liver parenchyma.

MRI technique

The MRI was performed using a 3T clinical scanner (Ingenia CX; Philips Healthcare, Best, the Netherlands) with a 32-channel phased-array receiver coil. Magnetic resonance imaging contrast enhancement was achieved by the intravenous administration of 0.025 mmol/kg body weight (0.1 mL/kg) of gadoteric acid (Eovist or Primovist; Bayer AG, Leverkusen, Germany) injected at a rate of 1 mL/s followed by a 30 mL saline flush at the same rate. All injections performed using a commercially available power injector.

The MRI protocol included the following sequences: breath-hold 2D dual-echo axial T_1 -weighted fast field-echo imaging (TR/TE, 234/2.4 ms in-phase and 234/1.2 ms opposed-phase); respiratory-triggered 2D fat-suppressed axial T_2 -weighted turbo spin-echo imaging (TR/TE_{eff}, 1,600/80 ms); and breath-hold gadoteric acid-enhanced hepatic arterial-, portal venous-, and late dynamic-phase imaging with a fat-suppressed 3D spoiled axial fast field-echo sequence (TR/TE, 3.3/1.6 ms; field-of-view, 42 × 29 cm; 320 × 320 image matrix [512 × 512 reconstruction]); parallel imaging factor, 1.6; flip angle, 15°; slice thickness, 4-mm section thickness with 2-mm overlap; and acquisition time, 20-s breath-hold for each phase comprising 90 slices.

Hepatobiliary phase imaging was initiated 20 min after the contrast injection. Image acquisition sets included fat-suppressed 3D T_1 -weighted turbo field echo (Cartesian) (eTHRIVE; Philips Healthcare) and FBRS acquisition (3D VANE; Philips Healthcare) (Fig. 1a).¹⁰ Three navigator echo-based respiratory compensation techniques are used in combination with FBRS. The navigator technique measures the position of the diaphragm by an additional quick MR pre-pulse before data collecting. During a scanning, the position of the diaphragm is automatically monitored. After the data acquisition completion, data only accepted when the position of the diaphragm falls within a gating window of 6 mm (gate technique). Furthermore, the position of the

acquired data is corrected according to the monitored diaphragm positions (track technique). These techniques are available individually or together (Fig. 1b).

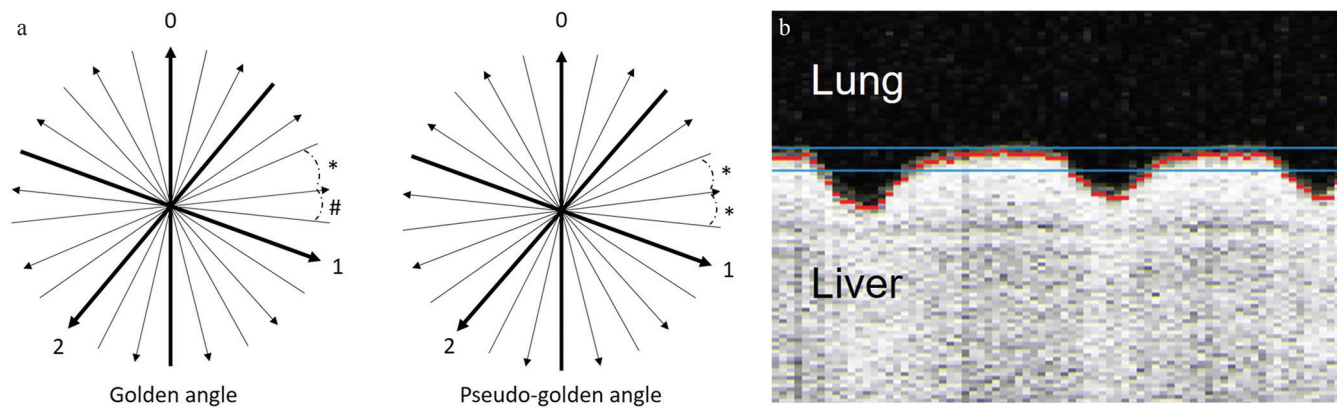
For each patient, the following six image acquisition sets were obtained in a random order: FBRS, FBRS with track (FBRS_T), FBRS with gate and track (FBRS_{G&T}), thin-slice FBRS with gate and track (thin-slice FBRS_{G&T}), free-breathing (Cartesian_{FB}) and breath-hold (Cartesian_{BH}) Cartesian acquisition (Fig. 1c). Basic and detailed parameters of the sequences, including slice thickness/overlap, acquisition time, gating window, and turbo field echo (TFE) factor are summarized in Tables 1 and 2.

Quantitative image analysis

Quantitative measurements conducted by a radiologist with 5 years of post-training experience in interpreting body MRI. The signal intensity of the liver parenchyma (SI_{Liver}) and paraspinal muscles ($SI_{Muscles}$) was measured by placing a circular ROI. The signal intensity of the liver parenchyma was calculated on the right anterior, right posterior, left internal, and left external lobe, avoiding intrahepatic blood vessels, and then averaging SI from all areas. Standard deviation (SD_{Liver}) was also determined by placing a circular ROI on the liver. The signal-to-noise ratio (SNR) and contrast-to-noise ratio (CNR) of the liver were calculated as SI_{Liver}/SD_{Liver} and $(SI_{Liver} - SI_{Muscles})/SD_{Liver}$ within ROI.

Qualitative image analysis

Image quality was independently evaluated regarding the sharpness of the liver edge, visibility of intrahepatic vessels, motion artifacts, and overall image quality by two radiologists (with 17 and 8 years of post-training experience in interpreting body MRI) in random order, and then in consensus. We modified the scoring system that was shown to have high interrater repeatability in the previous study.^{12,13} Qualitative scores were recorded on a 5-point scale, evaluating sharpness of the liver edge (1: non-identifiable with non-diagnostic level, 2: obscured with degraded but interpretable, 3: moderately blurred with some effect on diagnostic quality, 4: almost clear with no effect on diagnostic quality, and 5: clearly visible), visibility of intrahepatic vessels (1: non-identifiable with non-diagnostic level, 2: obscured with degraded but interpretable, 3: moderately blurred with some effect on diagnostic quality, 4: almost clear with no effect on diagnostic quality, and 5: clearly visible), motion artifacts (1: extensive motion artifact with non-diagnostic level, 2: severe motion artifact with image degraded but interpretable, 3: moderate motion artifact with some effect on diagnostic quality, 4: minimal motion artifact with no effect on diagnostic quality, and 5: no motion artifact), and overall image quality (1: unacceptable, 2: suboptimal, 3: acceptable, 4: good, and 5: excellent). Motion artifact was defined as a blurring to the phase-encoding direction and extending across the entire FOV, unlike truncation artifacts that diminish quickly away from the hepatic boundary or abdominal wall.



c

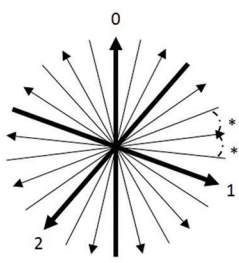
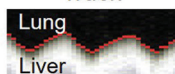
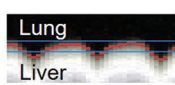
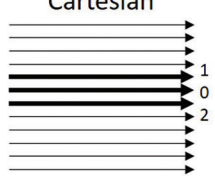
Schema of six image sets			
Image set	Breath hold	Data acquisition	Navigator technique
FBRs	No	Free-breathing pseudo-golden-angle radial stack-of-stars 	No
FBRs _T	No		Track 
FBRs _{G&T}	No		Gate and track 
thin-slice FBRs _{G&T}	No		
Cartesian _{FB}	Yes	Cartesian 	No
Cartesian _{BH}	No		No

Fig. 1 (a) Schema of pseudo-golden-angle radial stack-of-stars acquisition technique. Golden-angle radial stack-of-stars acquisition technique comprised radial k-space sampling spaced at a constant azimuthal increment of approximately 111.25° related to the golden ratio. This causes faint differences between angles (asterisk and pound). On the other hand, pseudo-golden angle technique adopted this angle with the added fine adjustment causing every radial lines be evenly spaced over time (asterisk). (b) Schema of the diaphragm navigation for Gate and track technique. Gate and track technique is a method to compensate the respiratory motion using three-navigator echo (x , y , and z -axis). The navigator technique measures the position of the diaphragm by an additional quick MR pre-pulse before data collecting. During a free-breathing scan, the position of the diaphragm is automatically monitored. After the data acquisition completion, data are accepted when the position of the diaphragm falls within a gating window (between blue lines) by gate technique. In track technique, the position of the acquired data is corrected according to the monitored diaphragm positions (red wavy line). These techniques are available individually or together. (c) Schema of six image sets. For each patient, the following six image acquisition sets were obtained in a random order: free-breathing pseudo-golden-angle radial stack-of-stars (FBRs), FBRs with track (FBRs_T), FBRs with gate and track (FBRs_{G&T}), thin-slice FBRs with gate and track (thin-slice FBRs_{G&T}), free-breathing Cartesian_{FB} and breath-hold Cartesian acquisition (Cartesian_{BH}).

Statistical analysis

Statistical analyses were performed using commercially available software (IBM SPSS Statistics, version 24.0; IBM Corporation, Armonk, NY, USA). Repeated measurements of analysis of variance were used to evaluate differences in

SI, SD, SNR, CNR among the six scan sequences. Qualitative scores also compared among sequences using Friedman’s test with the Wilcoxon signed-rank test for pairwise comparisons. A P -value of less than 0.05 considered statistically significant.

For a qualitative assessment of interobserver variability, kappa statistics used to measure the degree of agreement. A kappa value of up to 0.20 interpreted as slight agreement, 0.21–0.40 indicated fair agreement, 0.41–0.60 indicated moderate agreement, 0.61–0.80 indicated substantial agreement, and 0.81 or greater indicated almost perfect agreement.

Results

Patients

In the study period (November 2016 to January 2017), 63 consecutive patients received gadoteric acid-enhanced MRI. We excluded 13 of these patients based on the exclusion criteria. Hence, the study population included the remaining 50 patients (29 men and 21 women; age range, 27–84 years; mean age, 66.6 years). Among the 50 patients, 21 were diagnosed with viral hepatitis (17 patients with type C and 4 with type B), 18 with colorectal cancers, 6 with alcohol abuse, and 5 had abnormal ultrasounds but normal MRI. Twenty-one

patients with viral hepatitis classified into Child-Pugh class A in 18 patients and B in 3 patients.

Quantitative image analysis

Mean SI, SD, SNR, and CNR are summarized in Table 3 and Figs. 2–5. Liver parenchyma SI was significantly higher in FBRS, FBRS_T, FBRS_{G&T}, and thin-slice FBRS_{G&T} than in Cartesian_{FB} and Cartesian_{BH} ($P < 0.001$). SI in thin-slice FBRS_{G&T} (1508.9) was slightly lower than that in FBRS (1594.6), FBRS_T (1610.7), and FBRS_{G&T} (1611.2) ($P < 0.001$), but was significantly higher than that in Cartesian_{FB} (707.0) and Cartesian_{BH} (566.1) ($P < 0.001$; Fig. 2).

Liver parenchyma SD was significantly higher in FBRS, FBRS_T, FBRS_{G&T}, thin-slice FBRS_{G&T}, and Cartesian_{FB} than in Cartesian_{BH} ($P < 0.001$). SD in thin-slice FBRS_{G&T} (56.4) was significantly higher than that in FBRS (42.8), FBRS_T (43.8), FBRS_{G&T} (41.6), and Cartesian_{BH} (32.9) ($P < 0.001$) but was comparable with that in Cartesian_{FB} (50.4) ($P = 0.75$; Fig. 3).

Liver parenchyma SNR was significantly higher in FBRS, FBRS_T, FBRS_{G&T}, and thin-slice FBRS_{G&T} than in Cartesian_{FB} and Cartesian_{BH} ($P < 0.001$). Signal-to-noise ratio in thin-slice FBRS_{G&T} (32.0) was slightly lower than that in FBRS (42.8), FBRS_T (40.9), and FBRS_{G&T} (45.2) ($P < 0.001$), but was significantly higher than that in Cartesian_{FB} (16.3) and Cartesian_{BH} (19.5) ($P < 0.001$; Fig. 4).

Liver parenchyma CNR was significantly higher in FBRS, FBRS_T, FBRS_{G&T}, and thin-slice FBRS_{G&T} than in Cartesian_{FB} and Cartesian_{BH} ($P < 0.001$). Contrast-to-noise ratio in thin-slice FBRS_{G&T} (19.6) was slightly lower than that in FBRS (25.7), FBRS_T (23.2), and FBRS_{G&T} (26.5) ($P < 0.01$), but was significantly higher than that in Cartesian_{FB} (10.8) and Cartesian_{BH} (12.7) ($P < 0.001$; Fig. 5).

Qualitative image analysis

Based on sharpness of the liver edge, visibility of intrahepatic vessels, motion artifacts, and overall image quality, thin-slice FBRS_{G&T} had the highest image quality followed by Cartesian_{BH} and FBRS_{G&T} ($P < 0.001$; Table 4 and Fig. 6). Severe motion artifacts observed in 3 and 25 patients in Cartesian_{BH} and Cartesian_{FB}, respectively, whereas image quality remained over the acceptable range in FBRS_{G&T}, FBRS_T,

Table 1 Basic parameters for hepatobiliary phase imaging

	FBRS	Cartesian
TR / TE (ms)	3.8 / 1.64	3.3 / 1.57
Flip angle (°)	15	15
Field-of-view (mm)	420 × 420	420 × 294
Matrix (phase × frequency)	320 × 320 (recon 512)	320 × 320 (recon 512)
Band width (Hz/pixel)	620/0.701	620/0.701
Number of citations	1	1
Number of slices	90	90
Fat suppression	SPAIR	SPAIR
Reduction factor	1.5	1.6
Radial percentage (%)	120	–

FBRS: free-breathing pseudo-golden-angle radial stack-of-stars scan, SPAIR: spectral attenuated inversion recovery.

Table 2 Detailed parameters among six acquisitions

Scan sequences	Slice thickness/overlap (mm)	Acquisition time (sec)	Gating window (mm)	TFE factor
FBRS	4/–2	75	–	29
FBRS _T	4/–2	75	–	29
FBRS _{G&T}	4/–2	160.3 (96–250)	6	29
Thin-slice FBRS _{G&T}	2/0	256.6 (153–400)	6	58
Cartesian _{FB}	4/–2	16.8	–	46
Cartesian _{BH}	4/–2	16.8	–	46

Data in parentheses are ranges. FBRS, free-breathing pseudo-golden-angle radial stack-of-stars scan acquisition; FBRS_T, FBRS with track; FBRS_{G&T}, FBRS with gate and track; Cartesian_{FB}, free-breathing Cartesian acquisition; Cartesian_{BH}, breath-hold Cartesian acquisition; TFE, turbo field echo.

Table 3 Signal intensity of the liver among six sequences in 50 patients

Scan sequences	Signal intensity	Standard deviation	Signal-to-noise ratio	Contrast-to-noise ratio
FBRS	1594.6 ± 165.2	42.8 ± 14.1	42.8 ± 11.7	25.7 ± 8.2
FBRS _T	1610.7 ± 165.6	43.8 ± 12.1	40.9 ± 8.9	23.2 ± 7.4
FBRS _{G&T}	1611.2 ± 174.8	41.6 ± 13.5	45.2 ± 13.6	26.5 ± 8.4
Thin-slice FBRS _{G&T}	1508.9 ± 203.9	56.4 ± 22.0	32.0 ± 11.9	19.6 ± 7.7
Cartesian _{FB}	707.0 ± 228.9	50.4 ± 23.1	16.3 ± 4.7	10.8 ± 3.5
Cartesian _{BH}	566.1 ± 186.0	32.9 ± 13.0	19.5 ± 5.6	12.7 ± 4.1

Data are mean ± standard deviation (SD) scores. FBRS, free-breathing pseudo-golden-angle radial stack-of-stars scan acquisition; FBRS_T, FBRS with track; FBRS_{G&T}, FBRS with gate and track; Cartesian_{FB}, free-breathing Cartesian acquisition; Cartesian_{BH}, breath-hold Cartesian acquisition.

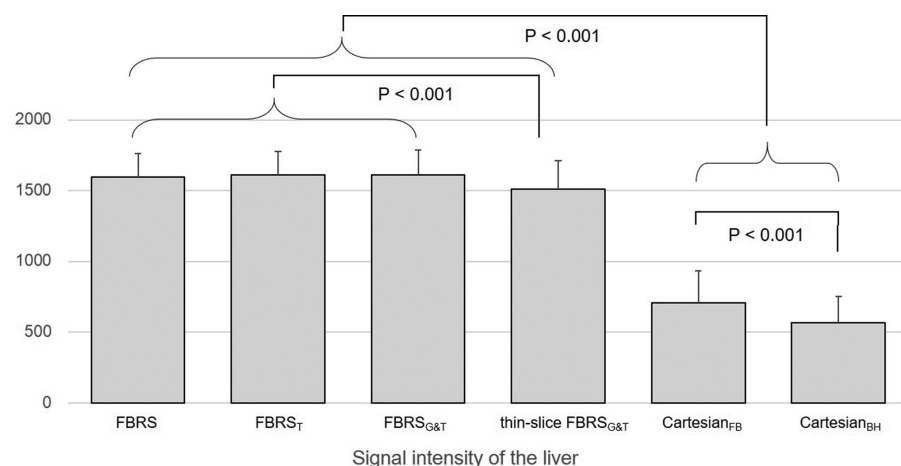


Fig. 2 Liver parenchyma signal intensity (SI) in hepatobiliary phase among six sequences. Liver parenchyma SI was significantly higher in free-breathing pseudo-golden-angle radial stack-of-stars (FBRS), FBRS with track (FBRS_T), FBRS with gate and track (FBRS_{G&T}), and thin-slice FBRS_{G&T} than in free-breathing Cartesian acquisition (Cartesian_{FB}) and breath-hold Cartesian acquisition (Cartesian_{BH}) ($P < 0.001$). SI in thin-slice FBRS_{G&T} (1508.9) was slightly lower than that in FBRS (1594.6), FBRS_T (1610.7), and FBRS_{G&T} (1611.2) ($P < 0.001$) but was significantly higher than that in Cartesian_{FB} (707.0) and Cartesian_{BH} (566.1) ($P < 0.001$).

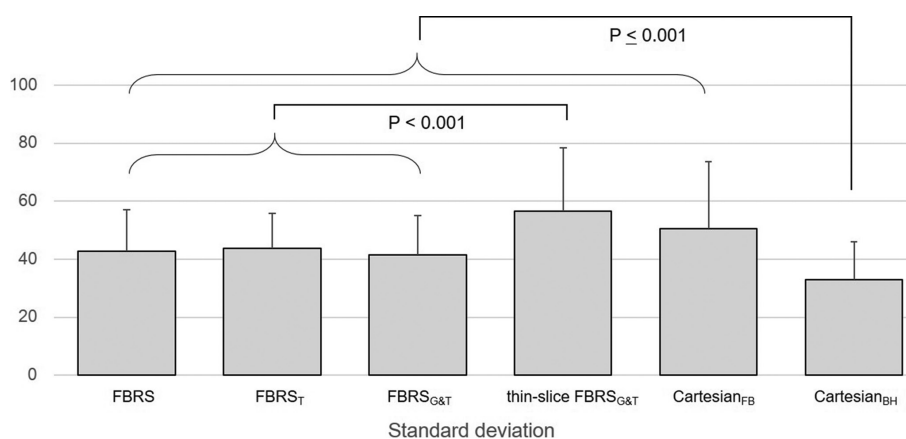


Fig. 3 Liver parenchyma standard deviation (SD) in hepatobiliary phase among six sequences. Liver parenchyma SD was significantly higher in free-breathing pseudo-golden-angle radial stack-of-stars (FBRS), FBRS with track (FBRS_T), FBRS with gate and track (FBRS_{G&T}), thin-slice FBRS_{G&T}, and free-breathing Cartesian acquisition (Cartesian_{FB}) than in breath-hold Cartesian acquisition (Cartesian_{BH}) ($P < 0.001$). SD in thin-slice FBRS_{G&T} (56.4) was significantly higher than that in FBRS (42.8), FBRS_T (43.8), FBRS_{G&T} (41.6), and Cartesian_{BH} (32.9) ($P < 0.001$) but was comparable with that in Cartesian_{FB} (50.4) ($P = 0.75$).

FBRS, and thin-slice FBRS_{G&T}. The kappa values of independent ratings for image quality by two observers ranged from 0.69 to 0.90, indicating substantial to almost perfect agreement.

Discussion

In traditional radial data acquisition techniques, the k -space sampled with equally spaced radial lines, all of which traverse the center of the k -space. We applied a free-breathing sampling technique, the FBRS acquisition technique, to

gadoteric acid-enhanced hepatobiliary phase imaging. This technique comprised radial k -space sampling spaced at a constant azimuthal increment of approximately 111.25° . This angle related to the golden ratio with the added fine adjustment and causes radial lines to be very evenly spaced over time.¹⁰ Our results demonstrate that FBRS achieved an almost three-fold increase in SI of liver parenchyma regardless of the slight increase in SD within ROI, resulting in an almost two-fold increase in SNR compared with conventional Cartesian data acquisition techniques. This strong SNR increase in the FBRS sequence may be necessary to

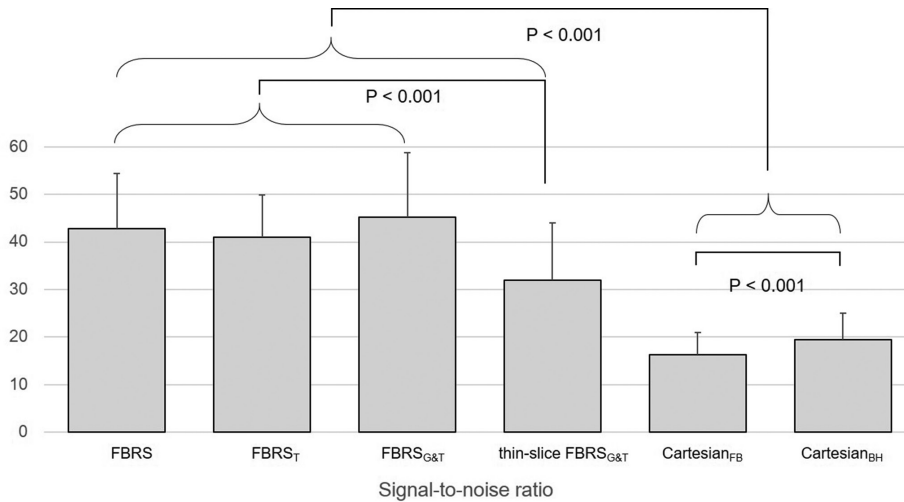


Fig. 4 Liver parenchyma signal-to-noise ratio (SNR) in hepatobiliary phase among six sequences. Liver parenchyma SNR was significantly higher in free-breathing pseudo-golden-angle radial stack-of-stars (FBRS), FBRS with track (FBRS_T), FBRS with gate and track (FBRS_{G&T}), and thin-slice FBRS_{G&T} than in free-breathing Cartesian acquisition (Cartesian_{FB}) and breath-hold Cartesian acquisition (Cartesian_{BH}) ($P < 0.001$). SNR ratio in thin-slice FBRS_{G&T} (32.0) was slightly lower than that in FBRS (42.8), FBRS_T (40.9), and FBRS_{G&T} (45.2) ($P < 0.001$) but was significantly higher than that in Cartesian_{FB} (16.3) and Cartesian_{BH} (19.5) ($P < 0.001$).

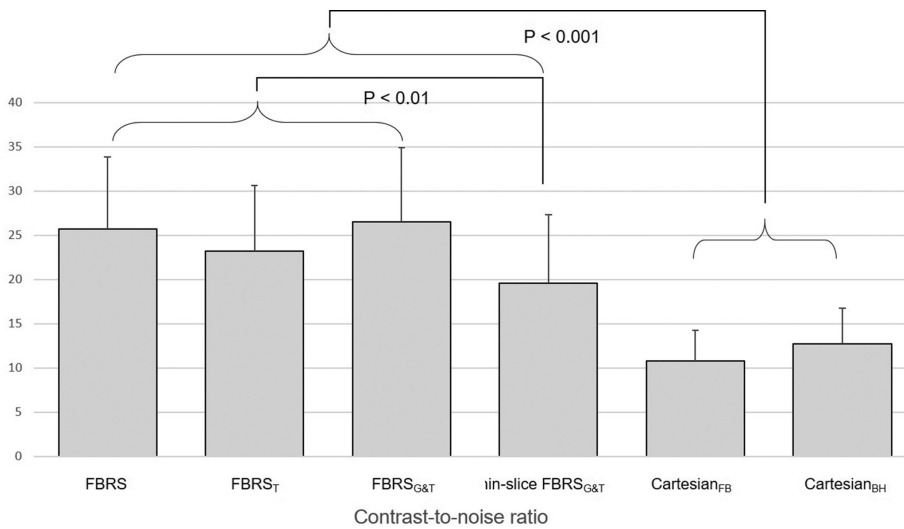


Fig. 5 Liver parenchyma contrast-to-noise ratio (CNR) in hepatobiliary phase among six sequences. Liver parenchyma signal-to-noise ratio (SNR) was significantly higher in free-breathing pseudo-golden-angle radial stack-of-stars (FBRS), FBRS with track (FBRS_T), FBRS with gate and track (FBRS_{G&T}), and thin-slice FBRS_{G&T} than in free-breathing Cartesian acquisition (Cartesian_{FB}) and breath-hold Cartesian acquisition (Cartesian_{BH}) ($P < 0.001$). SNR in thin-slice FBRS_{G&T} (19.6) was slightly lower than that in FBRS (25.7), FBRS_T (23.2), and FBRS_{G&T} (26.5) ($P < 0.01$) but was significantly higher than that in Cartesian_{FB} (10.8) and Cartesian_{BH} (12.7) ($P < 0.001$).

Table 4 Qualitative scores for six sequences in 50 patients

Scan sequences	Liver edge		Vessel		Motion artifact		Overall quality	
	Score	Significant difference	Score	Significant difference	Score	Significant difference	Score	Significant difference
FBRS	3.4 ± 0.6	3,4,5,6	3.5 ± 0.7	3,4,5,6	4.5 ± 0.7	3,4,5,6	3.6 ± 0.6	3,4,5,6
FBRS _T	3.4 ± 0.6	3,4,5,6	3.5 ± 0.7	3,4,5,6	4.5 ± 0.7	3,4,5,6	3.6 ± 0.6	3,4,5,6
FBRS _{G&T}	4.0 ± 0.6	1,2,4,5,6	3.8 ± 0.7	1,2,4,5	4.6 ± 0.6	1,2,4,5,6	4.0 ± 0.5	1,2,4,5
Thin-slice FBRS _{G&T}	4.6 ± 0.6	1,2,3,5,6	4.6 ± 0.7	1,2,3,5,6	4.8 ± 0.4	1,2,3,5,6	4.6 ± 0.6	1,2,3,5,6
Cartesian _{FB}	2.7 ± 0.7	1,2,3,4,6	2.3 ± 0.9	1,2,3,4,6	2.6 ± 0.8	1,2,3,4,6	2.5 ± 0.8	1,2,3,4,6
Cartesian _{BH}	4.2 ± 0.8	1,2,3,4,5	4.0 ± 0.9	1,2,4,5	4.1 ± 0.8	1,2,3,4,5	4.0 ± 0.8	1,2,4,5

Data are mean ± standard deviation (SD) scores. Significant differences are pairs that showed significant differences ($P < 0.05$) by pairwise comparisons. Numbers in significant difference, 1; FBRS, 2; FBRS_T, 3; FBRS_{G&T}, 4; Thin-slice FBRS_{G&T}, 5; Cartesian_{FB}, 6; Cartesian_{BH}. FBRS, free-breathing pseudo-golden-angle radial stack-of-stars scan acquisition; FBRS_T, FBRS with track; FBRS_{G&T}, FBRS with gate and track; Cartesian_{FB}, free-breathing Cartesian acquisition; Cartesian_{BH}, breath-hold Cartesian acquisition.

achieve high spatial resolution thin slice imaging with an effective slice thickness of 2 mm.

Taken together, FBRS sequences clearly reduced motion artifacts compared with Cartesian_{BH} sequences. Usually, the

movement of a scanned object during Cartesian k -space sampling causes characteristic ghosting motion artifacts in the phase-encoding direction.⁹ Because there is no phase-encoding direction during radial k -space sampling, FBRS

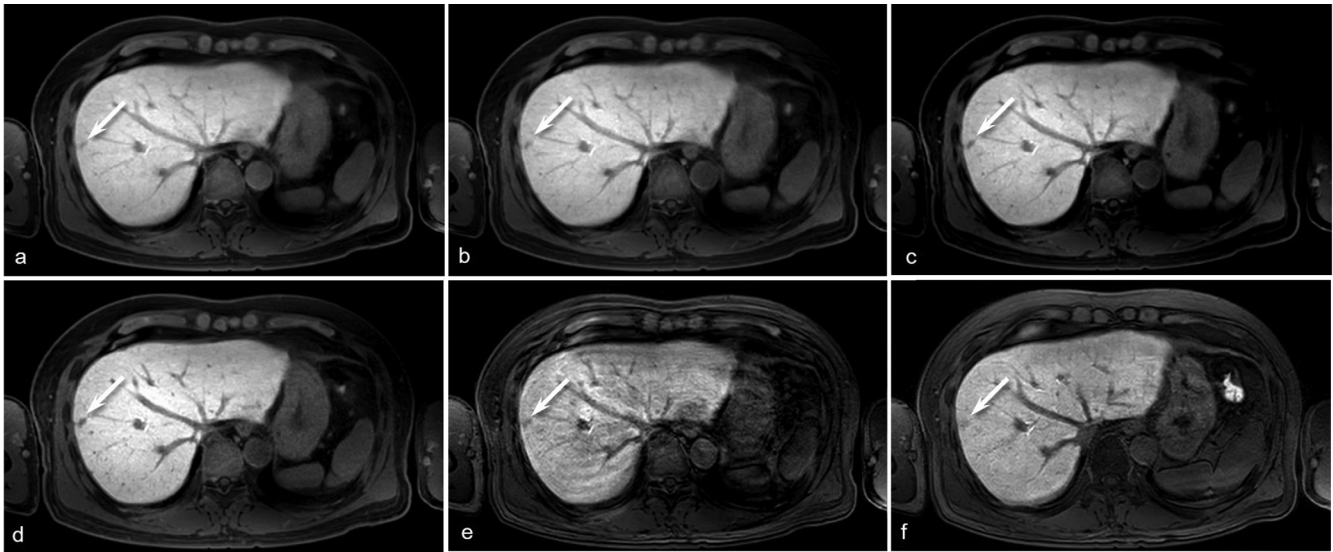


Fig. 6 An 59 year-old man with chronic hepatitis C and status post-radiofrequency ablation (RFA) for a hepatocellular carcinoma (HCC) in segment VII (a) free-breathing pseudo-golden-angle radial stack-of-stars (FBRS), (b) FBRS with track (FBRS_T), (c) FBRS with gate and track (FBRS_{G&T}), (d) thin-slice FBRS_{G&T}, (e) free-breathing Cartesian acquisition (Cartesian_{FB}), and (f) breath-hold Cartesian acquisition (Cartesian_{BH}). (a) demonstrated the slightly better image quality to (f) based on sharpness, motion artifacts, visibility of intrahepatic vessels, and overall image quality. Completely necrotic HCC status post-RFA appeared as a low signal intensity area in all sequences (arrow).

images are less affected by movement of the object being scanned. However, spatial resolution in the plane seemed slightly decreased in FBRS sequences compared with Cartesian_{BH} sequences based on qualitative scores of fine structures, such as sharpness of the liver edge and visibility of intrahepatic vessels. We assume this is because of a characteristic difference between the frequency components acquired by FBRS vs. Cartesian sequences. The radial sampling technique densely fills low-frequency components (central portion) in the k -space that affect the contrast resolution, whereas the Cartesian sampling technique fills the high-frequency component (peripheral portion), that affect spatial resolution, more fully than radial sampling. Regardless of this characteristic difference in data sampling, our qualitative results demonstrated excellent and significant improvements both in SNR and image quality in thin-slice FBRS_{G&T}, which makes imaging with thinner slices effective and resolves any disadvantages in image sharpness.

Contrary to these advantages above, prolongation of the acquisition time discussed as a fateful disadvantage in FBRS sequences compared with a very short acquisition time of 16.8 s in Cartesian sequences. Among the four free-breathing scans examined in our study, FBRS and FBTS_T were the simplest and fastest sequences because these two sequences keep filling the k -space data with limited influence of frequency and regularity of the breathing, resulting in the 75 s in acquisition time. Although the movement of the object less affected the radial sampling images, our qualitative results demonstrated the limitation of these two sequences in the overall image quality compared with Cartesian_{BH}. Consequently, the acquisition time was further extended (160 s in

FBRS_{G&T} and 256 s in thin-slice FBRS_{G&T}) by adding the gating technique that is a navigator technique measuring the position of the diaphragm and accepting the data only when the position of the diaphragm falls within a gating window. We believe it is necessary to make some substantial improvements in the free-breathing radial sampling sequence to shorten the acquisition time and to be a routine sequence in the liver MRI.

This study had some limitations. First, the number of patients examined was relatively small. Despite this, the FBRS acquisition technique had the best SNR and image quality compared with the conventional Cartesian_{BH} acquisition technique. Second, we did not evaluate diagnostic performance on focal hepatic lesions, although we believe that the excellent SNR and image quality of thin-slice FBRS images could yield better conspicuity of focal hepatic lesions. Third, we simply compared the FBRS and Cartesian acquisition without reference to the optimization of scan parameters, especially regarding FBRS, because we believe that each parameter should be carefully determined in each vendor or MR system. No parameters used in this study was specialized but vendor-recommended ones. Further study might be requested for the optimization of FBRS.

Conclusion

Thin-slice FBRS_{G&T} demonstrated excellent SNR and image quality compared with conventional breath-hold scans on gadoteric acid-enhanced hepatobiliary phase imaging. It can be apply to supplemental sequences to obtain good quality imaging in patients with unstable breath holding.

Conflicts of Interest

We have no known conflicts of interest associated with this publication and there has been no significant financial support for this work that could have influenced its outcome.

References

1. Reimer P, Schneider G, Schima W. Hepatobiliary contrast agents for contrast-enhanced MRI of the liver: properties, clinical development and applications. *Eur Radiol* 2004; 14:559–578.
2. Ahn SS, Kim MJ, Lim JS, Hong HS, Chung YE, Choi JY. Added value of gadoxetic acid-enhanced hepatobiliary phase MR imaging in the diagnosis of hepatocellular carcinoma. *Radiology* 2010; 255:459–466.
3. Kitao A, Zen Y, Matsui O, et al. Hepatocellular carcinoma: signal intensity at gadoxetic acid-enhanced MR Imaging—correlation with molecular transporters and histopathologic features. *Radiology* 2010; 256:817–826.
4. Narita M, Hatano E, Arizono S, et al. Expression of OATP1B3 determines uptake of Gd-EOB-DTPA in hepatocellular carcinoma. *J Gastroenterol* 2009; 44:793–798.
5. Tsuda N, Okada M, Murakami T. New proposal for the staging of nonalcoholic steatohepatitis: evaluation of liver fibrosis on Gd-EOB-DTPA-enhanced MRI. *Eur J Radiol* 2010; 73:137–142.
6. Sano K, Ichikawa T, Motosugi U, et al. Imaging study of early hepatocellular carcinoma: usefulness of gadoxetic acid-enhanced MR imaging. *Radiology* 2011; 261:834–844.
7. Woo JH, Song KD, Kim SH. Subcentimeter hypervascular nodules with typical imaging findings of hepatocellular carcinoma on gadoxetic acid-enhanced MRI: outcomes of early treatment and watchful waiting. *Eur Radiol* 2017; 27:4406–4414.
8. Goshima S, Kanematsu M, Kondo H, et al. Evaluation of optimal scan delay for gadoxetate disodium-enhanced hepatic arterial phase MRI using MR fluoroscopic triggering and slow injection technique. *AJR Am J Roentgenol* 2013; 201:578–582.
9. Chandarana H, Block KT, Winfeld MJ, et al. Free-breathing contrast-enhanced T1-weighted gradient-echo imaging with radial k-space sampling for paediatric abdominopelvic MRI. *Eur Radiol* 2014; 24:320–326.
10. Winkelmann S, Schaeffter T, Koehler T, Eggers H, Doessel O. An optimal radial profile order based on the golden ratio for time-resolved MRI. *IEEE Trans Med Imaging* 2007; 26:68–76.
11. Reiner CS, Neville AM, Nazeer HK, et al. Contrast-enhanced free-breathing 3D T1-weighted gradient-echo sequence for hepatobiliary MRI in patients with breath-holding difficulties. *Eur Radiol* 2013; 23:3087–3093.
12. Davenport MS, Vigiante BL, Al-Hawary MM, et al. Comparison of acute transient dyspnea after intravenous administration of gadoxetate disodium and gadobenate dimeglumine: effect on arterial phase image quality. *Radiology* 2013; 266:452–461.
13. Pietryga JA, Burke LM, Marin D, Jaffe TA, Bashir MR. Respiratory motion artifact affecting hepatic arterial phase imaging with gadoxetate disodium: examination recovery with a multiple arterial phase acquisition. *Radiology* 2014; 271:426–434.